Int. J. Microgravity Sci. Appl., 33 (3) (2016) 330308
DOI: 10.15011/jasma.33.330308

IIIII ISPS-6 Proceedings IIIII
(Original Paper)

Molecular Dynamics Simulations of Charge-Stabilized Colloidal Dispersions using the Sogami-Ise Potential

Yosuke KATAOKA

Abstract

Molecular dynamics simulations were carried out for charge-stabilized colloidal dispersions using the Sogami-Ise potential, based on general theoretical calculations of the electrostatic interaction in a macroionic solution. The molar weight of the particles was assumed to be 10000 g/mol, and the particle radius was 65 nm. The initial basic cell configuration was face-centered cubic (FCC) crystal, for which the number of particles N was 864. Periodic boundary conditions were assumed, and the cutoff length was the half of the cell length. The Gear integration method was used. An NTV ensemble was used, where V is the volume and the temperature T was 300 K. The liquid, FCC crystal and void structures were found. The obtained phase diagram is consistent with macroscopic observations and the results of Monte Carlo simulations of charge-stabilized colloidal dispersions.

Keyword(s): Molecular dynamics, Charge-stabilized Colloidal Dispersion, Sogami-Ise potential, Phase diagram
Received 18 September 2015, accepted 30 May 2016, published 31 July 2016.

1. Introduction

Charge-stabilized colloidal dispersions are known to exist as ordered phases under suitable conditions[1-6]. This phenomenon has frequently been studied on the basis of DLVO theory[7,8] as well as Sogami-Ise theory[9-11]. Tata and co-workers[12-16] also performed extensive Monte Carlo simulations of such systems. In the present work, molecular dynamics (MD) simulations[17-19] were performed to clarify the characteristics of various phases by determining thermodynamic quantities, pair distribution functions and self-diffusion coefficients associated with various molecular configurations and trajectories.

The phase diagram was obtained in (σ_n, ϕ) space where σ_n is the charge density on the surface of the colloidal particles and ϕ is the volume fraction. This phase diagram was compared with the experimental results obtained by Yamanaka[6].

In the last section of this paper, the phase boundary between the face-centered cubic (FCC) crystal and void phases is described in the case of a simple set of conditions with respect to the average interparticle distance and the distance that gives the minimum pair potential energy.

2. Molecular Dynamics Method

MD simulations[17-19] were performed to obtain the charge density and the volume fraction dependencies of the internal energy and pressure. In this study, the molecular interactions between spherical particles were assumed to be related to the Sogami–Ise potential[9-11].

The Debye screening factor κ is defined by the next formula:

$$\kappa^2 \equiv \frac{e^2}{\varepsilon k_B T V}\sum_j z_j^2 N_j \tag{1}$$

Here the usual notations are used: temperature T, volume V, unit charge e, dielectric constant of solvent ε, Boltzmann constant k_B, the charge of the jth small ions z_j, and number of particles of the jth small ions N_j.

Sogami–Ise potential $U^G(R)$ [9-11] expressed as a function of the center-to-center distance of particles R as in the following equation:

$$U^G(R) = \frac{Z^{*2}e^2}{\varepsilon}\left[\frac{1+\kappa a\coth(\kappa a)}{R} - \frac{1}{2}\kappa\right]e^{-\kappa R} \tag{2}$$

where

$$Z^* = Z\frac{\sinh(\kappa a)}{\kappa a} \tag{3}$$

Here the radius of the colloidal particles is a, and the net charge number of the colloidal particles is Z.

The DLVO pair potential $U^F(R)$ was also assumed for comparison, as below[11].

$$U^F(R) = \frac{Z^{*2}e^2}{\varepsilon}\frac{1}{R}e^{-\kappa R} \tag{4}$$

The parameters in the above equation are the same as those used for the Sogami–Ise potential.

Department of Chemical Science and Technology, Faculty of Bioscience and Applied Chemistry, Hosei University, 3-7-2 Kajino-cho, Koganei, Tokyo 184-8584, Japan.
(E-mail: yosuke.kataoka.7t@stu.hosei.ac.jp)

In both Eqs. (2) and (4), the van der Waals term is neglected because this term is negligible at low concentrations.

In these calculations, the molar mass of the particles was assumed to be 10,000 g/mol, and the particle radius a was 65 nm. The initial basic cell configuration was FCC crystal, with an N value of 864. Periodic boundary conditions were assumed and the cutoff length was half of the unit cell length. The Gear integration method was used with a time increment of 25 fs and the total duration of the molecular dynamics simulation was 50 ns. An NTV ensemble was used with T = 300 K, volume fraction ranging from 0.00001 to 0.1 and salt concentration C_s being 0 or 2 μM. The surface charge density σ_n was varied from 0.01 to 10 μC/cm^2. MD simulations were performed using the computational tool SCIGRESS-ME[20].

3. Molecular Dynamics Results

Typical results obtained from MD simulations for volume fraction ϕ of 0.03 showing the final configurations at charge densities σ_n of 0.05, 0.2 and 0.4 μC/cm^2 are presented in **Figs. 1**, **2** and **3**, respectively. **Figure 1** is assigned to a liquid structure, while the configuration in **Fig. 2** has an FCC structure and a void structure is seen in **Fig. 3**, although this image also shows an ordered region.

The self-diffusion coefficients D are calculated by the long-term part of the mean-square displacement[18]. These are plotted as functions of σ_n in **Fig. 4**. The value of D is very large in the range of $\sigma_n \leq 0.06$ μC/cm^2 and this range is identified with the liquid state. In the region defined by 0.07 μC/cm^2 $\leq \sigma_n \leq$ 0.35 μC/cm^2, the state is assigned to an FCC solid because of the small D and the regular configuration. The state in the range $\sigma_n >$ 0.4 μC/cm^2 is assigned to the void structure that is overall inhomogeneous containing the solid-like and gas-like regions. This phenomenon is best understood by considering the following figures.

In **Fig. 5**, the pair correlation functions $g(R)$ are plotted for the above three structures. The Wendt–Abraham parameter[21] is shown as functions of the charge density in **Fig. 6**. This parameter is defined as shown in EQ. (5). The first minimum $g(R)_{min}$ is divided by the first maximum $g(R)_{max}$. This parameter is small in an FCC structure shown in **Fig. 6**.

$$\text{Wendt–Abraham parameter} = \frac{g(R)_{\min}}{g(R)_{\max}} \qquad (5)$$

The average pair potential energies divided by the thermal energy values are presented in **Fig. 7**. In the FCC and void structures, the average potential energy is seen to decrease with increasing the charge density. This trend results from the deeper potential well associated with the greater charge density, as shown in **Fig. 8**. In the case of the void structure, the average potential energy is described by the following equation:

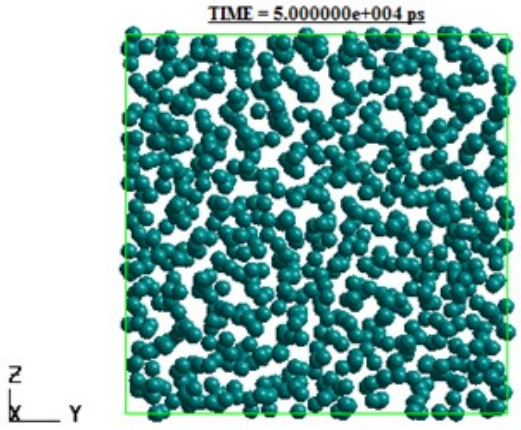

Fig. 1 An example of a liquid phase configuration at a charge density σ_n of 0.05 μC/cm^2, volume fraction ϕ of 0.03 and T = 300 K.

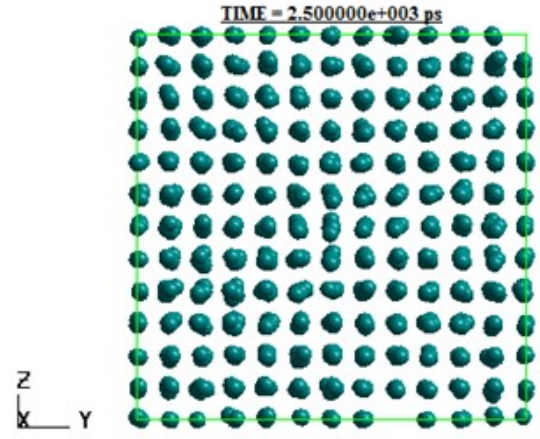

Fig. 2 An example of an FCC solid phase configuration at σ_n = 0.2 μC/cm^2, ϕ = 0.03 and T = 300 K.

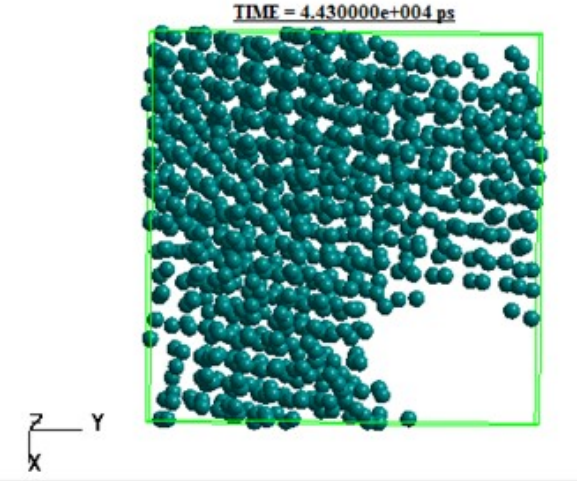

Fig. 3 An example of a void phase configuration at σ_n = 0.4 μC/cm^2, ϕ = 0.03 and T = 300 K.

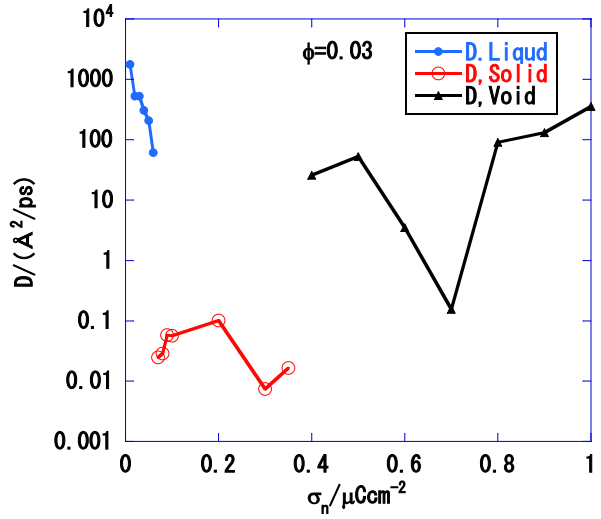

Fig. 4 Values of the self-diffusion coefficient D as functions of σ_n at $T = 300$ K.

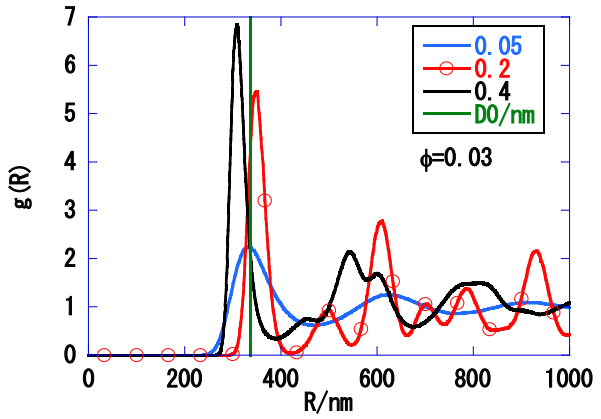

Fig. 5 Values of the pair correlation function $g(R)$ as functions of the molecular distance R. Three cases are shown: $\sigma_n = 0.05$, 0.2 and 0.4 μC/cm^2 at $\phi = 0.03$ and $T = 300$ K. The vertical line indicates the average distance D_0.

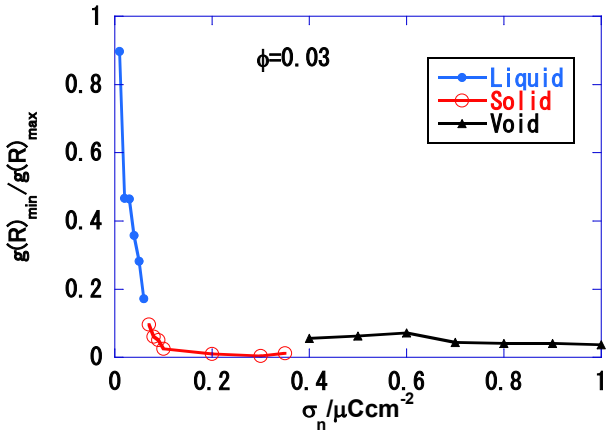

Fig. 6 Wendt–Abraham parameter as functions of σ_n at $\phi = 0.03$ and $T = 300$ K.

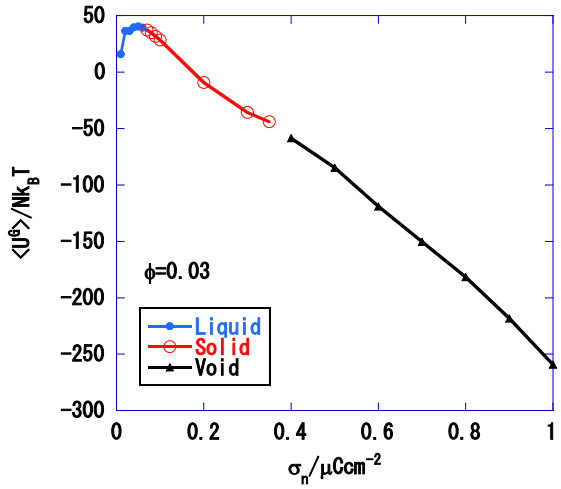

Fig. 7 The average of the potential energy normalized by the thermal energy $\langle U^G \rangle / NkT$ as functions of σ_n at $\phi = 0.03$ and $T = 300$ K.

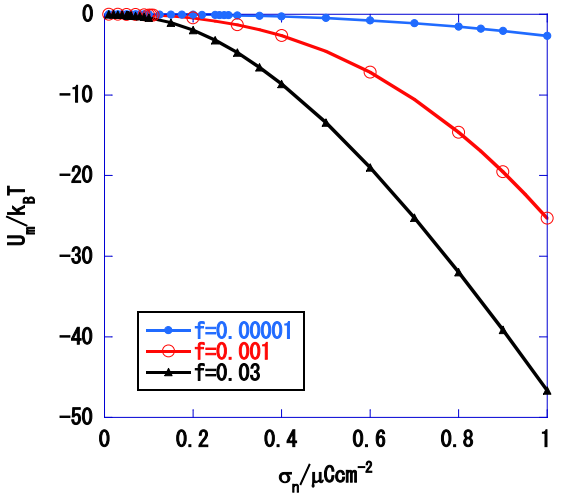

Fig. 8 The minimum value of the pair energy normalized by the thermal energy U_m/NkT as functions of σ_n. Three cases are shown: $\phi = 0.00001$, 0.001 and 0.03 at $T = 300$ K.

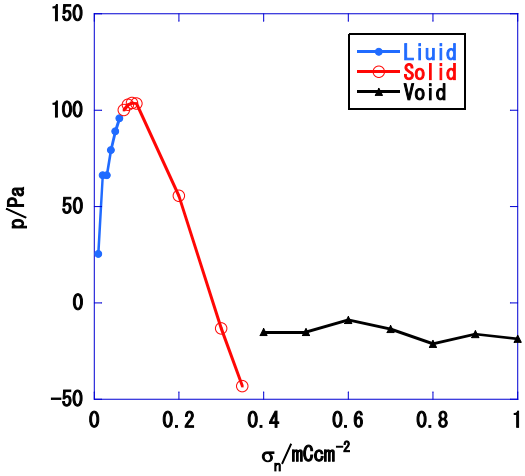

Fig. 9 Values of the pressure p as functions of σ_n at $\phi = 0.03$ and $T = 300$ K.

$$\left\langle U^G \right\rangle \approx \frac{z}{2} N U_m , \tag{6}$$

where z is the number of nearest neighbors.

The system pressures p are plotted as functions of charge density in **Fig. 9**. These pressure values equal the osmotic pressure[22] because the effective potential function between colloidal particles was employed, so the absolute value of the pressure is consistently very low.

4. Phase Diagram

The phase diagram obtained from these calculations is shown in **Fig. 10** in (σ_n, ϕ) space. With regard to the salt concentration, C_s, two scenarios were addressed: C_s = 0 and 2 μM. The same diagram is presented using a logarithmic scale for the volume fraction axis in **Fig. 11**. This phase diagram is consistent with that reported by Yamanaka[6]. The middle region of the diagram represents the FCC solid state, while the leftmost part corresponds to the liquid; both of these assignments are the same as those in Yamanaka's work[6]. In contrast, the rightmost region is assigned to a void structure in our case. Tata and coworkers described this void structure as a state in which gas and solid coexist[23-25], and this is also true with our MD simulation results, as shown in **Fig. 12**. Here, an example of trajectories is given for the void structure. In these trajectories, the solid-like and gas-like regions are also seen.

In **Fig. 13** the phase diagram calculated from DLVO potentials is compared with that derived using the Sogami-Ise (SI) approach. The FCC solid region in the DLVO diagram is much wider than in the case of the SI diagram. In addition, because the DLVO potential is always repulsive, no void structure appears, so the right hand region in this diagram is assigned to a random structure.

5. Structures

In order to understand the structures in the present colloidal particle system, it is helpful to compare the pair potential function, $U^G(R)$, and the pair correlation function $g(R)$. **Figure 14** shows this comparison in the case of the liquid structure (σ_n = 0.05 μC/cm^2, ϕ = 0.03). The $g(R)$ values exhibit a typical liquid phase curve, and the minimum distance R_m, of the $U^G(R)$ plot is greater than the position of the first peak in the $g(R)$ plot. These results differ from those expected for a normal liquid. The position of the first $g(R)$ peak corresponds to the average distance in the cell, D_0, as estimated from the following equation.

$$D_0 = \left(\frac{V}{N} \right)^{1/3} \tag{7}$$

The $g(R)$ function is shown in **Fig. 15** for the case of the FCC solid structure (σ_n = 0.2 μC/cm^2, ϕ = 0.03). The position of the

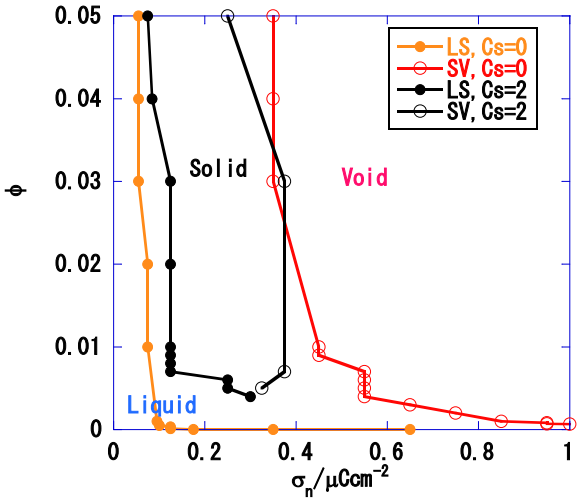

Fig. 10 The phase diagram obtained by MD simulations using the Sogami-Ise (SI) potential in (ϕ, σ_n) space at T = 300 K.

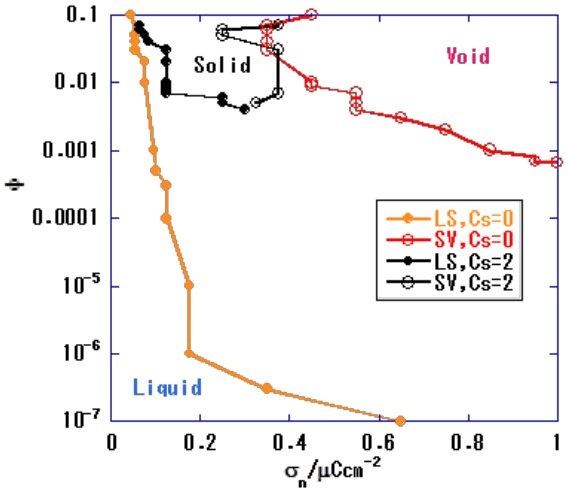

Fig. 11 The phase diagram obtained by MD simulations using the SI potential in (ϕ, σ_n) space, with the volume fraction axis on a logarithmic scale at T = 300 K.

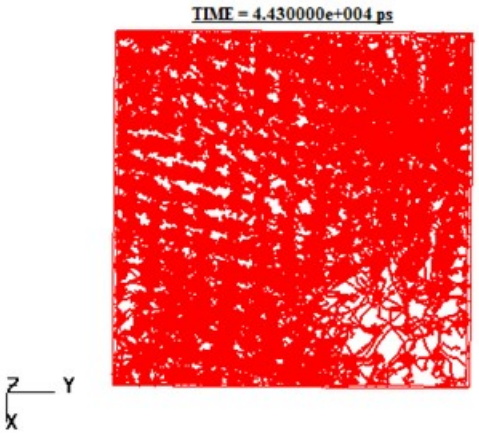

Fig. 12 An example of the trajectories in the void phase, for σ_n = 0.4 μC/cm^2, ϕ = 0.03 and T = 300 K.

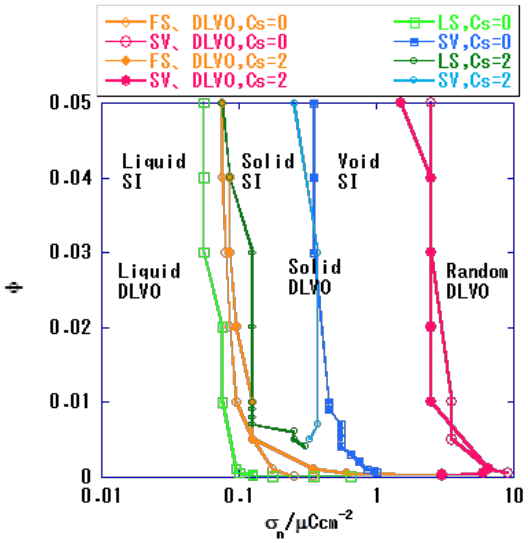

Fig. 13 The phase diagram obtained by MD simulations using the DLVO system in (ϕ, σ_n) space at T = 300 K. The SI system data are also shown.

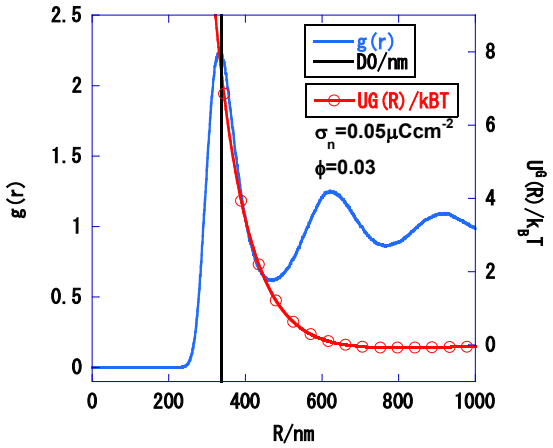

Fig. 14 The pair correlation function $g(R)$ and the pair potential energy $U^G(R)$ for the liquid structure as functions of R, at σ_n = 0.05 μC/cm^2, ϕ = 0.03 and T = 300 K. The vertical line indicates the average distance, D_0.

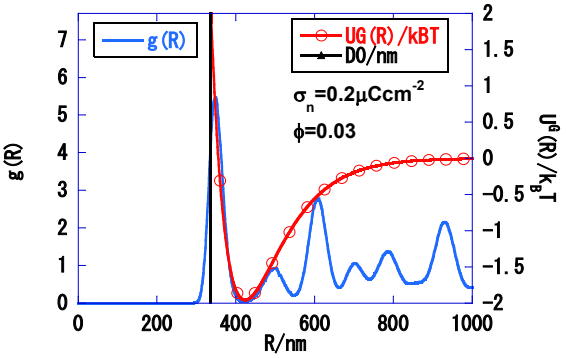

Fig. 15 The pair correlation function $g(R)$ and the pair potential energy $U^G(R)$ for the FCC structure as functions of R, at σ_n = 0.2 μC/cm^2, ϕ = 0.03 and T = 300 K. The vertical line indicates D_0.

first $g(R)$ peak corresponds to the average distance in the cell, D_0, which is associated with the repulsive part of the pair interaction. However, the average value $\langle U^G \rangle$ is negative, as was seen in **Fig. 7** and the pressure is positive but very small, as in **Fig. 9**. These findings can be understood by considering **Fig. 16**, which plots the running coordination number, $N(R)$. This figure shows that the coordination numbers in the vicinities of the third and fourth $g(R)$ peaks are larger than that of the nearest neighbor.

The data for the void structure is presented in **Fig. 17** (σ_n = 0.4 μC/cm^2, ϕ = 0.03). In this case, $U^G(R)$ is negative at the first peak position in the $g(R)$ plot, which is at a position less than the mean distance D_0. The plot of $g(R)$ indicates that this structure has solid-like regions.

6. Estimation of Transition Points

In the first part of this section, the transition between the FCC solid and void structures is estimated based on the distance of the minimum pair potential R_m. This distance decreases as the charge density increases, as shown in **Fig. 18**. If R_m is smaller than the mean distance D_0, this indicates that a stable pair is readily established in the cell, because the void structure appears from the excess space. In the case that R_m is greater than D_0, a close packed FCC structure is instead established with the aid of attractive interactions. The solution to the following equation with respect to charge density for a given volume fraction thus gives the transition point between the FCC solid and the void structure.

$$R_m(\sigma_n, \phi) = D_0(\phi) \tag{8}$$

In **Fig. 19**, the transition point is compared with that derived from MD simulations (**Figs. 10** and **11**), and the agreement is seen to be satisfactory.

In order to estimate the transition point between the liquid and the FCC solid, the MD results were analyzed. The value of the minimum pair energy U_m, divided by the thermal energy at the transition point is plotted as a function of the volume fraction in **Fig. 20**. The value of Um/k_BT is associated with the potential well depth of the pair energy. If this depth becomes sufficiently shallow, a transition takes place from the FCC solid to the liquid state under the condition of constant volume. From this plot, an empirical equation for the transition point between the liquid and the solid structures is obtained, as shown below.

$$\frac{U_m(\sigma_n, \phi)}{k_B T} = -0.089 \tag{9}$$

The results obtained from the above approach are compared with the data from MD simulations in **Fig. 21**. These plots demonstrate that the empirical equation estimates a reasonably accurate transition point in the region in which the volume fraction ϕ exceeds 0.0001.

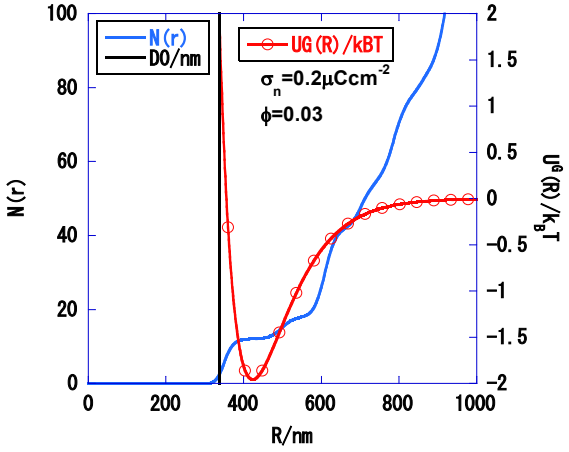

Fig. 16 The running coordination number $N(R)$ and the pair potential energy $U^G(R)$ for the FCC structure as functions of R, at σ_n = 0.2 μC/cm^2, ϕ = 0.03 and T = 300 K. The vertical line indicates D_0.

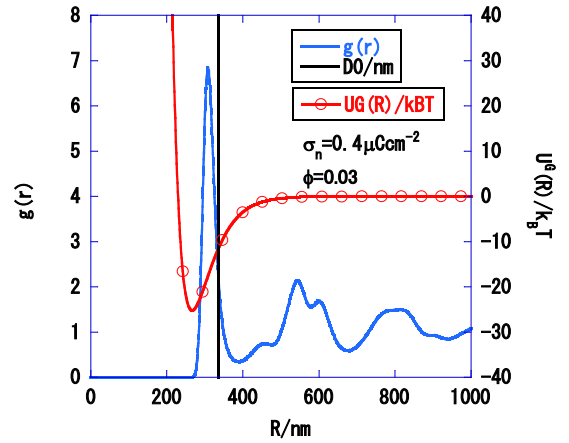

Fig. 17 The pair correlation function $g(R)$ and the pair potential energy $U^G(R)$ for the void structure as functions of R, at σ_n = 0.4 μC/cm^2, ϕ = 0.03 and T = 300 K. The vertical line indicates D_0.

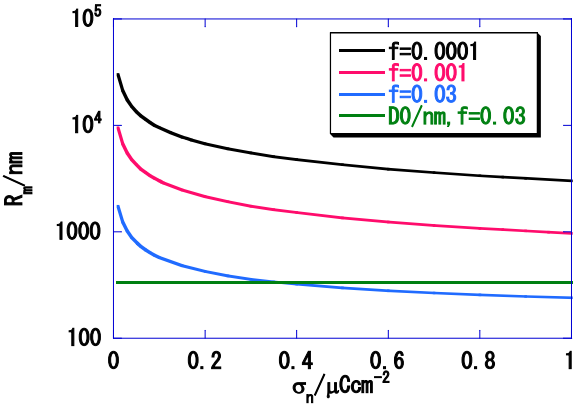

Fig. 18 The distances at the potential minimum (R_m) as functions of σ_n. Three cases are shown: ϕ = 0.0001, 0.001 and 0.03 at T = 300 K. The horizontal line indicates D_0 at ϕ = 0.03.

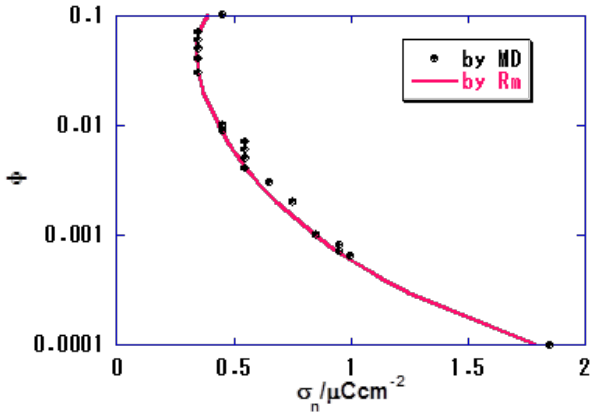

Fig. 19 The transition volume fraction ϕ between the solid and void structures calculated using Eq. (8) as a function of σ_n at T = 300 K. The values obtained from MD simulations are also shown for comparison.

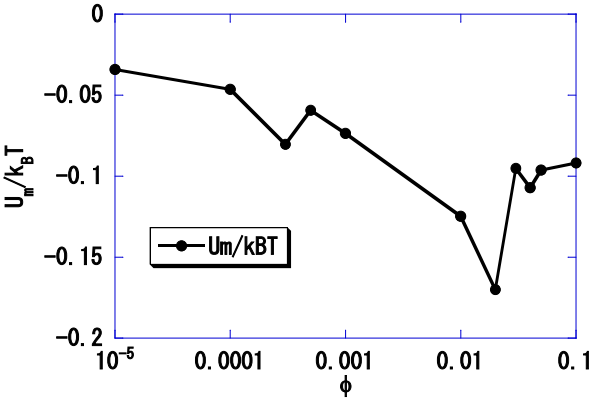

Fig. 20 The minimum potential energy normalized by the thermal energy U_m/k_BT at the transition between the liquid and solid phases as a function of ϕ at T = 300 K.

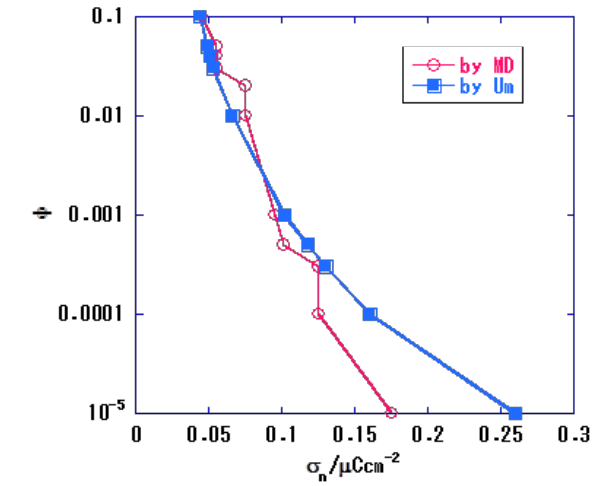

Fig. 21 The transition volume fraction ϕ between the liquid and solid phases calculated using Eq. (9) as a function of σ_n at T = 300 K. The values obtained from MD simulations are also shown for comparison.

7. Experiments under Microgravity

To confirm validity of the Sogami-Ise theory, we are planning experiments of structure analyses of colloidal dispersions of high density particles such as SiO_2 and TiO_2 by laser diffraction and CCD photography in the Kibo module of ISS[26]. The most important points are observations on phase transition from the FCC crystal to the void structure according to the increasing surface charge density. The appearance of the void structure is the expected evidence of the attractive interaction because only random structure appears for the case of large surface charge density in the repulsive system like DLVO dispersion as shown in **Fig. 13**.

8. Conclusions

The phase diagram of a charge-stabilized colloidal dispersion was obtained by MD simulations using the Sogami-Ise potential. This diagram is consistent with both macroscopic observations and the results of Monte Carlo simulations of charge-stabilized colloidal dispersions. The dispersion structures and the nature of the phase transitions were discussed based on the interparticle distance and the energy of the minimum pair potential. The reason why the void structure appears is elucidated by the attractive interaction.

Acknowledgments

The author would like to thank the Research Center for Computing and Multimedia Studies of Hosei University for the use of computer resources.

References

1) S. Hachisu, Y. Kobayashi, and A. Kose: J. Colloid Interface Sci., **42** (1973) 342.
2) A.K. Arora and B.V.R. Tata: Ordering and Phase Transitions in Charged Colloids, VCH, New York (1996).
3) Y. Monovoukas and A. P. Gast: J. Colloid Interface Sci., **128** (1989) 553.
4) T. Palberg, W. Mönch, F. Bitzer, R. Piazza and T. Belloni: Phys. Rev. Lett., **74** (1995) 4555 .
5) J. Yamanaka, T. Koga, N. Ise and T. Hashimoto: Phys. Rev., **E 53** (1996) R4317.
6) J. Yamanaka, H. Yoshida, T. Koga, N. Ise and T. Hashimoto: Phys. Rev. Lett., **80** (1998) 5806.
7) V. Derjaguin and L. Landau: Acta Physicochim., USSR, **14** (1941) 633.
8) E.J.W. Verwey and T.G. Overbeek: Theory of the Stability of Lyophobic Colloids, Elsevier (1948).
9) I. Sogami: Phys. Lett., **96A** (1983) 199.
10) I. Sogami and N. Ise: J. Chem. Phys., **81** (1984) 6320.
11) N. Ise and I. S. Sogami: Structure Formation in Solution, Springer (2005).
12) B.V.R. Tata and N. Ise: Phys. Rev., **B 54** (1996) 6050.
13) B.V.R. Tata, E. Yamahara, P. V. Rajamani and N. Ise: Phys. Rev. Lett., **78** (1997) 2660.
14) B.V.R. Tata and N. Ise: Phys. Rev., **E 58** (1998) 2237.
15) N. Ise, T. Konishi and B.V.R. Tata: Langmuir, **15** (1999) 4176.
16) P.S. Mohanty and B.V.R. Tata: J. Colloid Interface Sci., **264** (2003) 101.
17) M.P.Allen and D.J. Tildesley: Computer Simulation of Liquids, Clarendon Press, Oxford (1992).
18) R.J. Sadus: Molecular Simulation of Fluids, Theory, Algorithms and Objective-Orientation, Elsevier, Amsterdam (1999).
19) Y. Kataoka: Int. J. Microgravity Sci. Appl., **32** (2015) 320208.
20) http://www.scigress.com/ (accessed 2015).
21) H.R. Wcndt and F.F. Ahraham: Phys. Rev. Lett., **41** (1978) 1244.
22) I.S. Sogami, M.V. Smalley, and T. Shinohara: Prog. Theor. Phys., **113** (2005) 235.
23) B.V.R. Tata, P.S. Mohanty, J. Yamanaka, and T. Kawakami: Mol. Sim., **30** (2004) 153.
24) P.S. Mohanty, B.V.R. Tata, A. Toyotama and T. Sawada: Langmuir, **21** (2005) 11678.
25) B.V.R. Tata and S. Jena: Solid State Communications, **139** (2006) 562.
26) I.S. Sogami: ISPS-6/ITTW2015, 16Col-1K, 14-18 September (2015).